Cell

Structure of the Rigor Actin-Tropomyosin-Myosin Complex

Elmar Behrmann,[1] Mirco Müller,[2] Pawel A. Penczek,[3] Hans Georg Mannherz,[1,4] Dietmar J. Manstein,[2,*] and Stefan Raunser[1,*]

[1]Department of Physical Biochemistry, Max Planck Institute of Molecular Physiology, 44227 Dortmund, Germany
[2]Institute for Biophysical Chemistry, Hannover Medical School, 30625 Hannover, Germany
[3]Department of Biochemistry and Molecular Biology, The University of Texas, Houston Medical School, Houston, TX 77030, USA
[4]Department of Anatomy and Molecular Embryology, Ruhr-University, 44801 Bochum, Germany
*Correspondence: manstein.dietmar@mh-hannover.de (D.J.M.), raunser@mpi-dortmund.mpg.de (S.R.)
http://dx.doi.org/10.1016/j.cell.2012.05.037

SUMMARY

Regulation of myosin and filamentous actin interaction by tropomyosin is a central feature of contractile events in muscle and nonmuscle cells. However, little is known about molecular interactions within the complex and the trajectory of tropomyosin movement between its "open" and "closed" positions on the actin filament. Here, we report the 8 Å resolution structure of the rigor (nucleotide-free) actin-tropomyosin-myosin complex determined by cryo-electron microscopy. The pseudoatomic model of the complex, obtained from fitting crystal structures into the map, defines the large interface involving two adjacent actin monomers and one tropomyosin pseudorepeat per myosin contact. Severe forms of hereditary myopathies are linked to mutations that critically perturb this interface. Myosin binding results in a 23 Å shift of tropomyosin along actin. Complex domain motions occur in myosin, but not in actin. Based on our results, we propose a structural model for the tropomyosin-dependent modulation of myosin binding to actin.

INTRODUCTION

Muscle contraction and many other motile processes such as cell motility, endocytosis, or cytokinesis are mediated by the interaction of members of the myosin superfamily with actin filaments. ATP binding and hydrolysis by myosin trigger a sequence of conformational changes that are associated with an approximately 10,000-fold change in actin affinity. In turn, actin binding promotes the successive release of phosphate (P_i) and ADP. The movement of myosin along actin filaments is thought to be caused by large conformational changes associated with the release of the hydrolysis products. Rapid rebinding of ATP leads to myosin dissociation from the filament and initiates a new cycle (Figures 1A and 1B). This mechanochemical reaction cycle, first described by Lymn and Taylor (1971), was later extended to greater detail, including several weakly and strongly bound states of the actomyosin complex (Sweeney and Houdusse, 2010). It has only been partially characterized at the structural level. Crystal structures of myosin motor domains in the absence or presence of nucleotides or nucleotide analogs provide detailed insights into states, in which myosin is dissociated from the actin filament (Figure 1A) (Coureux et al., 2004; Houdusse et al., 2000). However, because the complex of filamentous (F)-actin with myosin (Figure 1A) is refractory to crystallization, structural information on the actin-myosin complex was only obtained at medium resolution from X-ray fiber diffraction (Huxley et al., 1980; Irving et al., 2000) and cryo-electron microscopic (cryo-EM) studies (Holmes et al., 2003; Rayment et al., 1993; Volkmann et al., 2003). The highest resolution obtained so far for a three-dimensional (3D) cryo-EM reconstruction was 14 Å and allowed the rigid-body fitting of actin and myosin crystal structures (Holmes et al., 2003). Along with spectroscopic studies and crystal structures of myosin II and Va motor domains in the absence of nucleotide (Conibear et al., 2003; Coureux et al., 2003; Reubold et al., 2003), this reconstruction strongly suggests that myosin closes its so-called 50 kDa cleft upon binding to F-actin. This conformational change is coupled to the opening of the nucleotide-binding pocket in a manner that is not yet fully understood.

In the basic functional unit of striated muscle, the sarcomere, actin, and myosin filaments are arranged in parallel and slide past each other to cause shortening. The interaction of myosin with actin is controlled by the actin-binding proteins tropomyosin and troponin (Ebashi et al., 1969). At low Ca^{2+} concentrations, troponin locks tropomyosin in a position on F-actin where it obstructs the myosin-binding site, thus preventing contraction of the sarcomere (Lehman et al., 1995). When Ca^{2+} binds to troponin, tropomyosin moves azimuthally on the actin filament, in this way exposing the myosin-binding site. Myosin attaches to the actin filament and performs a power stroke, which results in shortening of the sarcomere. So far, the only structural information on the interaction of actin, myosin, troponin, and tropomyosin is a cryo-EM reconstruction at 26–30 Å by Milligan and Flicker (1987). A better mechanistic description of the interaction of actin and myosin and its regulation by tropomyosin requires a spatial resolution, at which secondary structure elements of proteins can be identified directly, i.e., subnanometer resolution.

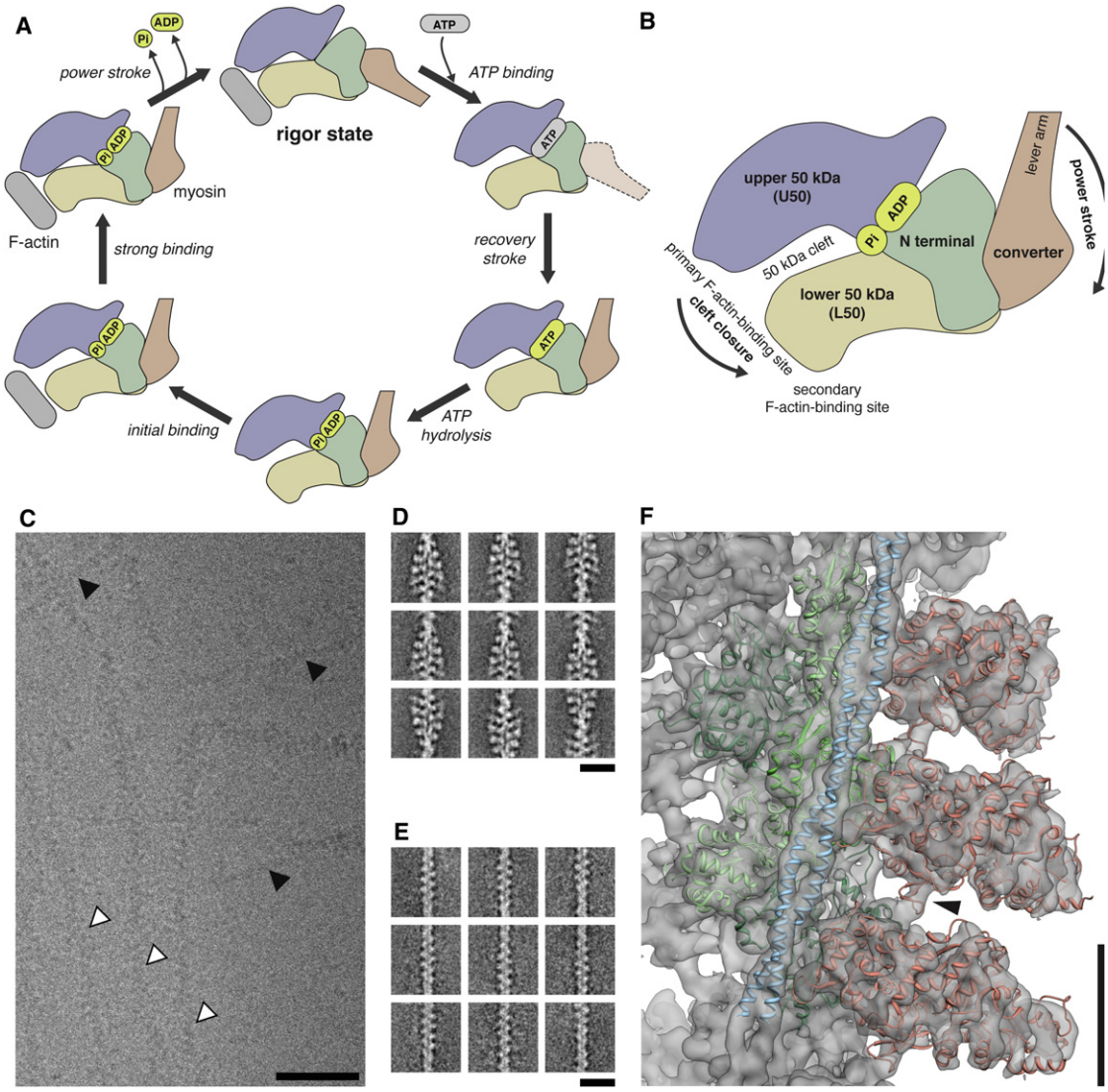

Figure 1. Actomyosin ATPase Cycle and Cryo-EM of F-Actin and the Complex of F-Actin, Tropomyosin, and the MyoE Motor Domain

(A) Scheme of the actomyosin ATPase cycle is illustrated.

(B) Schematic overview of myoE subdomains is shown.

(C) Subarea of an unprocessed image of the vitrified sample recorded at a defocus of 1 μm is demonstrated. The presence of a mixture of two filament types is evident (decorated filaments marked by white arrowheads; undecorated filaments marked by black arrowheads). Filaments appear to be either decorated or undecorated over their complete length. Scale bar, 50 nm.

(D) Representative class averages of the decorated filaments (35,374 segments) are presented. No classes with partial decoration were identified. Scale bar, 20 nm.

(E) Representative class averages of the undecorated filaments (4,629 segments) are illustrated. No classes with partial decoration were identified. Scale bar, 20 nm.

(F) Fit of pseudoatomic model into the electron density map of the ATM complex is shown. Central subunits are depicted as ribbon traces of the Cα coordinates. MyoE, actin, and tropomyosin are salmon, light green, and blue, respectively. Arrowhead indicates the contact between myoE and actin −2. Scale bar, 5 nm. See also Figure S1.

Here, we report the first subnanometer-resolution structure of the actin-tropomyosin-myosin complex in the rigor (nucleotide-free) state determined by cryo-EM. The pseudoatomic model of the complex, obtained from fitting crystal structures into the map, defines a large actin-myosin-tropomyosin interface. This interface involves two adjacent actin monomers and one tropomyosin pseudorepeat per myosin motor domain contact. Hydrophobic interactions that were not predicted from MD simulations, as well as potential salt bridges and electrostatic interactions, define a strong contact between myosin and actin. Due to this interaction, the proteins are interlocked in a cogwheel-like manner. Furthermore, we provide structural

evidence for direct interactions between myosin and tropomyosin in the complex. The actin-myosin interface creates a neutral groove with positively charged patches that can optimally accommodate negatively charged areas on tropomyosin. The critical importance of the tight interaction of all three proteins is further supported by the fact that several mutations in cardiac β-myosin or α-actin isoforms resulting in severe forms of familial hypertrophic cardiomyopathy (CM) map to the actin-myosin-tropomyosin interface. By comparing the rigor (nucleotide-free) and prepower stroke (ADP/P_i-bound) state of actin, tropomyosin, and myosin, we discovered that binding of myosin results in a shift of tropomyosin along the actin filament and conformational changes in myosin, but not in actin. Notably, the closure of the 50 kDa cleft is mediated mostly by a 16° rotation of the upper 50 kDa (U50) subdomain of myosin. Finally, we propose a structural model for tropomyosin-dependent myosin binding to actin and for actin-induced nucleotide release from myosin.

RESULTS AND DISCUSSION

Structure Determination and Overall Architecture

Because the F-actin-tropomyosin-myoE (ATM) complex is most stable in the rigor state, with the nucleotide-free myosin strongly bound to tropomyosin-decorated F-actin (Figure 1A), we chose to work with the complex in this state. By screening many combinations of F-actins and myosin motor domains, we searched for filaments that would work best for EM (fully decorated, straight, stiff, and not bundled). The combination of rabbit skeletal muscle F-actin with the motor domain of *Dictyostelium discoideum* myosin-IE (Kollmar et al., 2002) (myoE), a fast single-headed molecular motor that is involved in the phagocytic uptake of solid particles, bacteria, and yeast cells (Dürrwang et al., 2006), proved to be the best specimen for this study. The addition of skeletal muscle tropomyosin, which wraps around the F-actin filament, improved the rigidity of the filaments even further. We observed that actin filaments were either fully decorated with myosin and tropomyosin or did not bind the proteins at all (Figures 1C–1E). This suggests that tropomyosin and myosin have a higher affinity to the F-actin-myosin and F-actin-tropomyosin complex, respectively, than to F-actin alone. These findings are in good agreement with previous studies showing that the myosin motor domain subfragment 1 (S1) binds to F-actin-tropomyosin filaments with a 7-fold higher affinity than to undecorated F-actin (Geeves and Halsall, 1986) and that myosin increases the actin affinity of tropomyosin (Eaton, 1976).

We collected cryo-EM images and analyzed them as described in Experimental Procedures. After separation of the data into two sets for either decorated or nondecorated filaments (Figures 1D and 1E), we determined 3D cryo-EM structures of both F-actin alone and the ATM complex at a resolution of 8.9 and 7.7 Å, respectively (Figure 1F; see Figures S1A and S1E available online). For the ATM complex, we determined in total three different structures from the same data set that differed mainly in the regions most distant from the helical axis (see also Experimental Procedures and Figures S1B–S1D).

The pseudoatomic model of F-actin obtained from a previously published cryo-EM study by Fujii et al. (2010) and the atomic model of myoE by Kollmar et al. (2002) were then fit into the electron densities (Figures 1E and S1). Because no crystal structure of the full tropomyosin complex has been obtained, we used a previously published tropomyosin model that was created based on crystal structures of subfragments, low-resolution EM data, and its optimal electrostatic fit to actin (Li et al., 2011). In this way, we obtained a pseudoatomic model of the complete ATM complex that defines the molecular interactions between the partner proteins.

Actin-Myosin Interface

Our pseudoatomic model clearly shows that myosin interacts with two adjacent actin molecules via several loops forming a large contact surface (1,820 $Å^2$). Whereas loop 2, and helix HW, loop 4 and the CM loop of myoE form large contacts to SD1 and SD3 of the neighboring actin molecule (actin 0), loop 3 attaches to SD1 of the next lower actin along the long pitch helix. In addition, a helix-loop-helix motif of the lower 50 kDa (L50) subdomain of myosin protrudes into a cavity formed by SD1 and SD3 of the upper and by the SD2 domain of the lower actin (actin −2), thereby interacting with both of them (Figures 2, 3A, and S2; Movie S1). By examining the hydrophobic surface potentials, it becomes obvious that both the helix-loop-helix motif and the cavity are predominantly hydrophobic (Figure 3B). In addition, two clusters of hydrophobic residues on the CM loop interact with hydrophobic regions on actin (29–31, 329–334). As shown before, these hydrophobic stretches are important for maintaining the strong binding state of myosin (Sasaki et al., 1999). Their critical importance for a tight binding is further supported by the fact that mutations in the genes encoding cardiac β-myosin or α-actin isoforms that result in myopathies map to hydrophobic regions of the ATM interface (Figure 3E; Table S1).

In contrast, the contacts between other regions of the actin-myosin interface are mostly mediated by electrostatic interactions and potentially involve the formation of salt bridges (Figures 2B, 2C, and 3C; Movie S2). Salt bridge formation appears to contribute to the formation of a double sandwich composed of the highly negatively charged N terminus of actin (D1, E2, D3, E4), a conserved positively charged region in myoE loop 2 and on helix HW (K556, K557, R558, R567), a negatively charged loop from actin SD1 (residues 20–28 [D24, D25]), and conserved positively charged residues on the myoE CM loop (R323, K331, R332) (Figures 3C, 3D, and S3A). The importance of these charged residues has been shown previously. MyoE residue R332 corresponds to human β-cardiac myosin R403, which is associated with a severe form of familial hypertrophic CM when mutated to glutamine (Figure 3E; Table S1) (Geisterfer-Lowrance et al., 1990). Mutation of D25 to asparagine in skeletal α-actin causes one of the most severe forms of the congenital, hereditary neuromuscular disorder nemaline rod myopathy (Figure 3E; Table S1) (Sparrow et al., 2003). The two conserved lysines at the C-terminal end of myosin loop 2 (K652/K653 in smooth muscle myosin II and K556/K557 in myoE) are necessary for triggering actin activation. The net charge and charge density of loop 2 greatly affect actin affinity and for nonprocessive myosins, actin-activated ATPase activity (Furch et al., 1998; Joel et al., 2001).

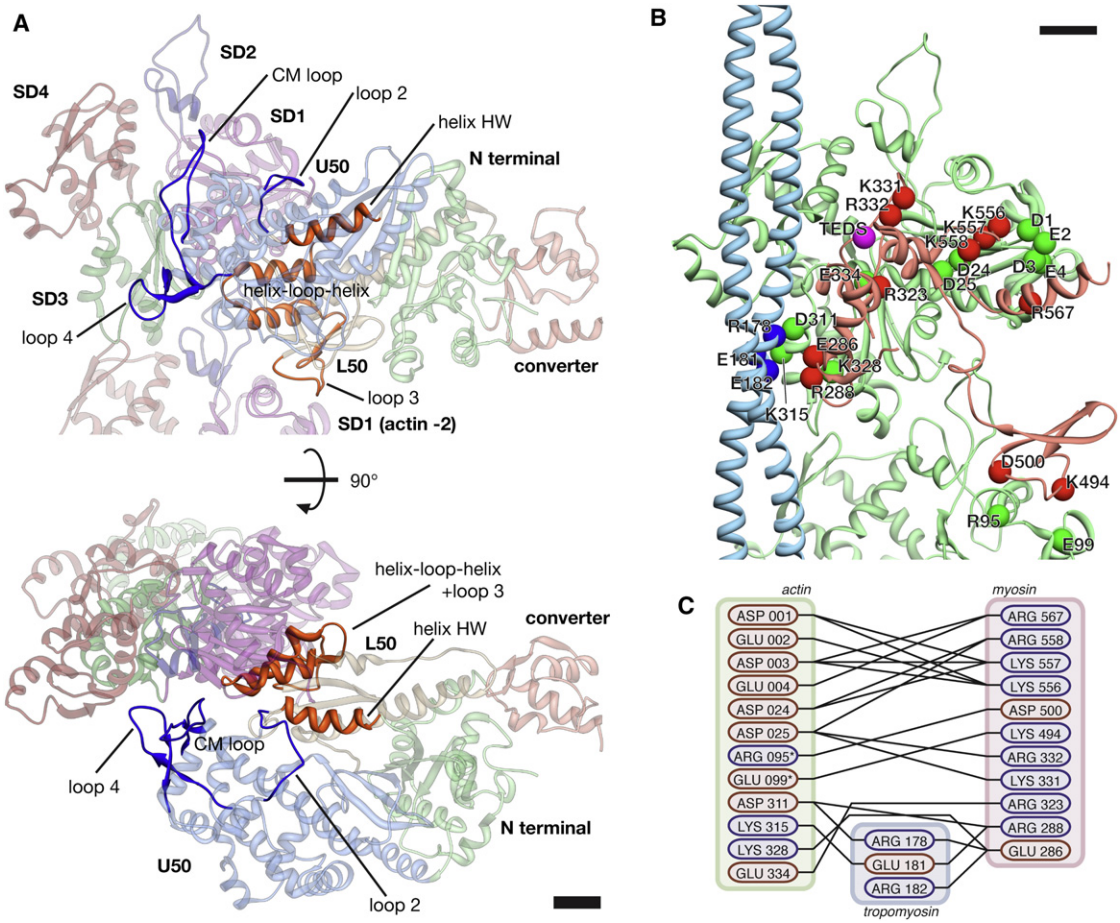

Figure 2. The Binding Interface with Potential Key Electrostatic Interactions among Myosin, Tropomyosin, and Actin 0 and −2

(A) Overview of the binding interface between myosin and actin from side and top view is shown. Regions on myosin involved in actin binding are highlighted and labeled: loop 2 (547–561), helix HW (563–577), loop 3 (482–501), loop 4 (278–298), CM loop (322–342), and helix-loop-helix motif of the L50 subdomain (445–481).

(B) Pseudoatomic model of the complete binding interface is presented. Potential interaction partners with complementary charges in close proximity are depicted as colored spheres. In addition the TEDS site (which is not part of the interface) is depicted as a pink sphere. The interface between actin 0 and myosin extends over 1,450 Å^2, the interface between actin −2 and myosin over 370 Å^2, the interface between actin 0 and tropomyosin over 210 Å^2, and the interface between myosin and tropomyosin over 300 Å^2.

(C) Cartoon representation of the interface is illustrated. Residues are colored by charge at pH 7.4. Asterisk denotes residues that are part of the actin −2 interface. For tropomyosin only residues of repeat V are depicted.

Scale bars, 1 nm.

See also Figures S2 and S3 and Movies S1 and S2.

Loop 2 sits not only in the middle of the described double sandwich but also at the center of the major actin-myosin interface. Our results shed light on the contribution of the actin N-terminal part to the actin-myosin interaction. It is well known that negative charges at the N-terminal part of actin are of critical importance for the ATP-dependent actin-myosin interaction (Miller et al., 1996), especially for weakly bound actomyosin states (Hansen et al., 2000). Remarkably, the N-terminal part is one of the few regions of actin that is not highly conserved (Figures 3C and 3D).

Our data also help to understand the role of the conserved TEDS site (S334, in our structure mutated to E334 to mimic phosphoserine; see also Experimental Procedures), which is located in the CM loop. As becomes obvious from our model, the side chain of E334 is not oriented toward actin but stabilizes the CM loop through interaction with the neighboring residue K332. This type of interaction was suggested earlier by comparing the crystal structure of the unphosphorylated myoE wild-type motor domain, where the CM loop is disordered, to structures of other myosins with a glutamate or aspartate residue at this position (Kollmar et al., 2002).

It was shown that residues D460, E461, and A462 on the myosin helix-loop-helix motif are important for the myosin-actin interaction (Furch et al., 2000; Giese and Spudich, 1997). Although these conserved residues are at the actin-myosin interface in our model, there are no obvious complementary charges on the actin surface. It is therefore more likely that the negative charges in this region are important for stabilizing myosin

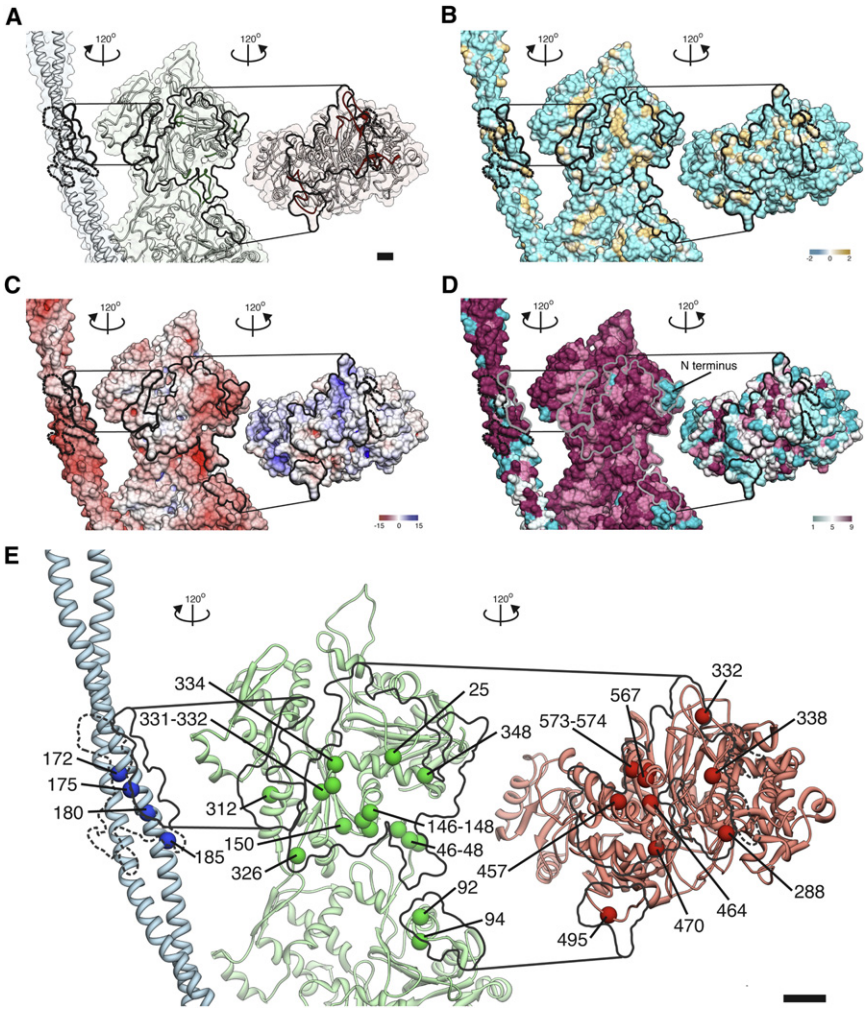

Figure 3. Binding Interfaces between F-Actin, MyoE, and Tropomyosin and Mapping of Residues Responsible for Myopathies when Mutated in Human Proteins

Tropomyosin has been rotated 120° clockwise and shifted to the left, whereas myosin has been rotated 120° counterclockwise and shifted to the right. Interfaces were calculated and are delimited by lines drawn onto the surfaces.

(A) Overview of the complex is presented. Important loops of actin and myosin are highlighted to help with orientation.

(B) Calculated surface hydrophobicity potential is demonstrated. Hydrophobic patches are colored orange.

(C) Calculated surface electrostatic potential at pH 7.2 is illustrated. Positive-charge density is colored blue, and negative-charge density is red. Both tropomyosin and actin appear largely negatively charged, whereas the interface site of myosin is dominated by positive charges.

(D) Surface map colored by residue conservation score is presented. Conserved residues are shown in pink. Actin and tropomyosin are highly conserved, whereas the interface site of myosin only contains a few conserved residues.

(E) Pseudoatomic model of the complete binding interface with residues that are associated with myopathies, when mutated in human cardiac actin, tropomyosin, and myosin depicted as colored spheres is shown. For tropomyosin only residues of repeat V are depicted.

Scale bars, 2 nm.

See also Table S1 and Movies S1 and S2.

loop 2 (R567) by electrostatic interactions. This would also explain the observed effect of charge-modifying mutations on actin affinity (Furch et al., 2000).

Earlier studies suggested an additional stabilization of the actomyosin complex by interaction of loop 3 with the SD2 of actin −2 (Milligan, 1996; Rayment et al., 1993; Schröder et al., 1993). Our cryo-EM structure confirms that this contact exists (Figure 1F). Based on our model, we can show how salt bridges may contribute to this contact (Figures 2B and 2C). Biochemical experiments indicate that loop 3-mediated contacts are not a feature shared between all myosin isoforms (Van Dijk et al., 1999). Their presence in the complex formed by myoE and F-actin may contribute together with other factors, such as the lack of an SH3-like N-terminal domain, to the well-ordered and straight appearance of the decorated filaments used in our study. Despite local differences, basic features of the complex described here are shared with other types of myosins. The motor domain is the most conserved region of myosin. Only minor structural differences are observed in the polypeptide backbone positions of myoE and myosin II (Kollmar et al., 2002). Differences are restricted to the nature of side chains in less well-conserved regions, and the length and composition of surface loops. In comparison to similar myosins, these loop regions appear to be actually more constrained than the sequences of the rest of the myosin molecule (Goodson et al., 1999).

From Prepower Stroke to Rigor State

The previously observed intrastrand crosslinking of actin filaments indicated that structural transitions in actin are necessary for actomyosin force generation (Kim et al., 2002). To identify putative conformational changes in F-actin that result from myosin binding to the actin filament, we compared F-actin models derived from undecorated with myoE-decorated actin filaments (Figures 4A–4C and S4A–S4H). We superposed the atomic models of an undecorated (Figure S1A) and decorated F-actin subunit (Figures 1F and S1D) and determined the root-mean-square deviations (rmsds) between the carbon-α positions (Figures 4A and 4B). The low rmsds indicate that conformational changes are minimal and distributed over the whole structure. The strongest differences were localized in the region of the DNase I-binding loop and near the N terminus. This was also corroborated by eigenanalysis using a set of different F-actin models (Figures 4C and S4A–S4H). Besides their direct influence on force generation, conformational changes in this region may

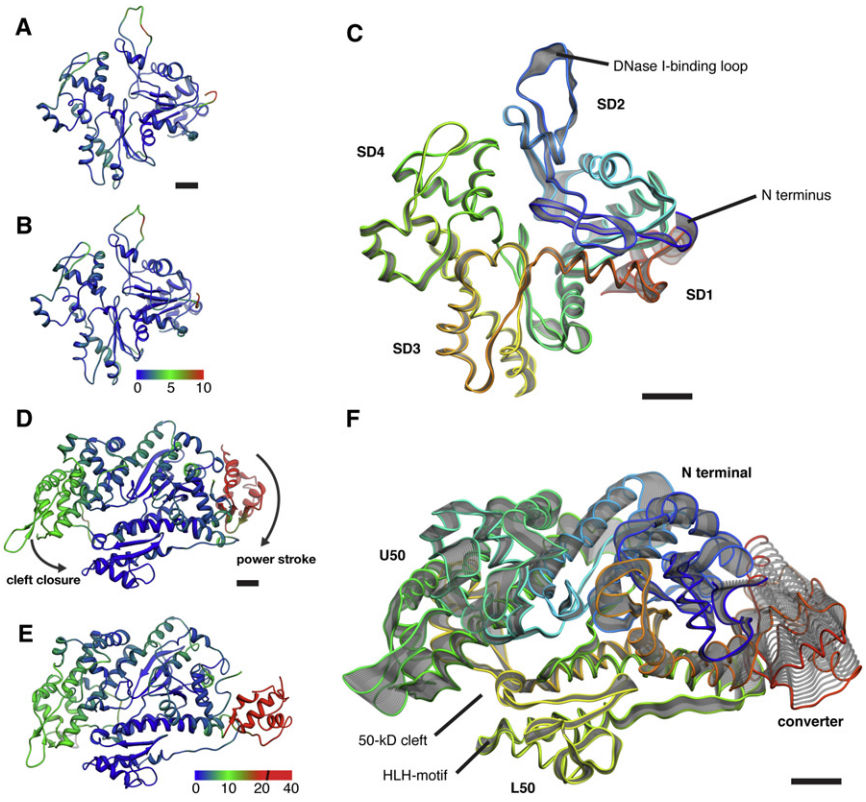

Figure 4. Conformational Changes between Prepower Stroke and Rigor State

Analysis of the variability of F-actin (A–C) and myoE (D–F) between prepower stroke (undecorated) and rigor (decorated) state is illustrated. (A and B) Atomic models of an undecorated (Figure S1A) and decorated F-actin subunit (Figures 1D and S1D), respectively, were reduced to α carbon positions only, superposed, and the rmsd was determined. Models are color coded by Cα rmsd values ranging from 0 Å (blue) to 10 Å (red). Major differences are found in the carboxy-terminal region of the DNase I-binding loop (residues 39–52) and the amino terminal region (residues 1–5). (C) We performed an eigenanalysis using the published models of F-actin (Fujii et al., 2010; Oda et al., 2009) (PDB 2ZWH and 3MFP), our undecorated actin model (Figure S1A), and our three models of actin decorated with myosin and tropomyosin (Figures S1B–S1D). Depicted is the visualization of the first eigenvector as a trajectory of SD-scaled displacements from the average structure. No clear pattern of displacements is discernable. Actin is colored with a rainbow gradient from blue (amino terminus) to red (carboxyl terminus). (D and E) Atomic models of myosin in the prepower stroke (PDB 1LKX, chain C) and rigor state (Figure 1D) were reduced to α carbon positions only, superposed, and the rmsd was determined. Models are color coded by Cα rmsd values in the range of 0–20 Å. In the converter domain, displacements ranged up to 40 Å. The second-highest displacement locates to the U50 subdomain. (F) We performed an eigenanalysis using the four available models of myoE in the nucleotide-bound state (Kollmar et al., 2002), actin-unbound state (PDB 1LKX, chains A–D), and our three models of nucleotide-free, actin-bound myoE (Figures S1B–S1D). Depicted is the visualization of the first eigenvector. Although the L50 subdomain, especially the helix-loop-helix motif, is almost invariable, clear changes are seen in all other subdomains indicating closure of the 50 kDa cleft and rotation of the converter domain. Myosin is colored with a rainbow gradient from blue (amino terminus) to red (carboxyl terminus). Scale bar, 1 nm.
See also Figures S4 and S5 and Movie S3.

be responsible for the observed cooperativity of tropomyosin and myosin binding (Figure 1). Interestingly, when we comparing our F-actin model with previously published F-actin models (Fujii et al., 2010; Oda et al., 2009), we observed the highest variability in the DNase I-binding loop and the region next to the N terminus, whereas the remaining regions of actin are almost invariable (Figures S4J–S4O). Therefore, we cannot rule out that the observed differences between undecorated and decorated F-actin are caused by a higher flexibility of these F-actin regions, as described for F-actin (Galkin et al., 2010; Splettstoesser et al., 2011). However, based on the lack of an SH3-like domain in myoE, which had been implicated in the cooperative binding of myosin heads to F-actin based on its role in mediating the formation of contacts between adjacent myosin heads (Schröder et al., 1993), we can now exclude that head-to-head contacts are important for the cooperativity of F-actin decoration by myosin motor domains.

By comparing our model for myoE in the rigor state (Figures 1A and 1F) with the structure of myoE in the ATP state (PDB 1LKX, chain C) (Figure 1A) (Kollmar et al., 2002), where myosin does not bind to actin, we identified conformational changes in myoE that result from its binding to the actin filament (Figures 4D and 4E). The cleft that separates the L50 and U50 subdomains in the unbound myosin in the prepower stroke state closes upon binding to actin by a 16° rotation of the U50 subdomain. As expected, the N terminal and the converter domain undergo large transitions, resulting in a swing of the lever arm by ~70° (Figures 4D and 4E; Movies S3 and S4). The same regions of variability were also found by eigenanalysis of the four available models of myoE in the nucleotide-bound state (Kollmar et al., 2002), actin-unbound state (PDB 1LKX, chains A–D), and our three models of nucleotide-free, actin-bound myoE (Figures S1B–S1D, 4F, and S5A–S5F). Interestingly, the L50 subdomain shows only little movement. This indicates that this subdomain is the site for the initial weak binding of myosin to actin, whereas the U50 subdomain interacts with actin only upon closure of the 50 kDa cleft, resulting in the formation of the full actomyosin-binding site and strong binding of myosin. As perceived from our ATM model, the contact between the L50 subdomain and actin is mainly based on hydrophobic interactions, whereas the large interface between the U50 subdomain and actin is predominantly supported by electrostatic contacts. In fact, the weak binding state is, in contrast to the strong binding state, not affected by ionic strength but can be disrupted by organic solvent (Geeves and Halsall, 1986). This indicates that mainly hydrophobic and

hydrophilic interactions contribute to the weak and strong binding state, respectively.

Myosin motor domains can be crystallized in their nucleotide-free state, as shown for chicken myosin V (Coureux et al., 2003) and *Dictyostelium* myosin II (Reubold et al., 2003). Despite the absence of F-actin, the 50 kDa cleft is closed in these structures. We compared our pseudoatomic model of myoE with the structure of the myosin V motor domain in the nucleotide-free state (Coureux et al., 2003) and found that they are quite similar. This indicates that this crystal structure indeed represents the strong binding conformation of myosin (Figures S3B–S3E). In both models, the central β sheet takes on the more twisted conformation compared to the respective postrigor and prepower stroke structures (Figures S3D and S3E). Whereas the U50 and L50 subdomains overlay fairly well, there are some differences in the HG, SH1, and SH2 helices and the converter domain (Figures S3B and S3C). Compared to other regions of the myosin motor, the converter domain and closely associated structural elements, such as the SH1 and SH2 helices, display increased mobility or greater variability in orientation in structurally well-accessible states of the ATPase cycle.

Rigor Does Not Mean Rigid

The F-actin models as well as the tropomyosin models obtained from the three ATM reconstructions (Figures S1B–S1D) differ only marginally (Figures S4I and S4P–S4U). The myoE models, however, show major differences in the U50 subdomain and especially in the converter domain when the three ATM reconstructions (Figures S1B–S1D) are compared (Figures S5G–S5L; Movie S4). This suggests that myosin displays conformational flexibility even when it is tightly bound to F-actin, as previously reported by Klein et al. (2008). Interestingly, high variability was also observed in the region of the converter domain when the four conformers of the myoE prepower-stroke crystal structure (Kollmar et al., 2002) were compared (Figures S5M–S5R). This indicates that flexibility of the converter domain is an intrinsic property of myoE. Remarkably, the movement of the converter domain does not result in a movement of the lever arm in the direction of the power stroke, but in a lateral movement perpendicular to the axis of the actin filament. If we assume a high rigidity of the myosin tail, this flexibility could be important for a proper interaction of myosin with F-actin because it allows the myosin head to be azimuthally rotated with respect to the actin filament.

Tropomyosin in the M State

Skeletal muscle tropomyosin is an ~40-nm-long α-helical coiled-coil protein that winds around the actin filament. Overlaps between the N and C termini of adjacent tropomyosins occur at every seventh actin, leading to the formation of a continuous rope-like structure. Tropomyosin is divided into seven pseudo-repeating units, each of which binds to a successive actin monomer along F-actin. Because these units are very similar and not distinguishable at a resolution of ~8 Å, we applied the helical symmetry of actomyosin to achieve maximal resolution but at the same time accepting that the overlap region of the N and C termini will not be visible in the maps.

Our electron densities show clearly two separated rod-like features that correspond to the two α helices of the tropomyosin coiled-coil winding around the actomyosin complex (Figures 1F and S1B–S1D). It becomes obvious from both our structure and model that tropomyosin fits nicely into the groove between actin and myosin (Movie S2). This shape complementarity, referred to as Gestalt binding, was described by Holmes and Lehman as a necessary prerequisite for the specific actin-tropomyosin interaction (Holmes and Lehman, 2008). In addition the complex is stabilized by electrostatic interactions between myosin and tropomyosin. Myosin loop 4 acts as a central linker that can interact with both actin and tropomyosin via salt bridges (Figures 2 and S2). Myopathy-causing mutations of tropomyosin at the ATM interface either remove one of the charged residues involved in salt bridge formation or cause charge reversal, thereby perturbing the proper interaction of the proteins in the ATM complex (Figure 3E; Table S1C).

In muscle thin filaments, three different positions of tropomyosin are presumed to exist. At low Ca^{2+} concentrations, troponin holds tropomyosin in the B (blocked) position. When Ca^{2+} levels increase, troponin allows tropomyosin to azimuthally move by ~25° to adopt the C (closed) state that allows initial myosin binding to actin. Myosin binding induces a further ~10° shift to the M (open) position (McKillop and Geeves, 1993; Vibert et al., 1997). It has long been deliberated whether tropomyosin slides or rolls over actin when changing between the different states. A rolling mechanism would imply that tropomyosin is a rather flexible molecule, whereas a more rigid-body-like behavior would be required for a sliding movement. Although the observation of systematic solvent exposure changes across specific stretches of the tropomyosin surface supports a rolling model (Holthauzen et al., 2004), the low twisting stiffness of tropomyosin and its cooperative behavior favor a sliding movement (Li et al., 2010).

Using low-resolution EM structures and computational chemistry, Li et al. identified a position of tropomyosin on F-actin with optimal electrostatic complementarity (Li et al., 2011). They postulated this to be its preferred position in the absence of troponin or other constraints (Li et al., 2011) (Figure 5). Because this position covers the myosin-binding sites on actin SD3 and part of actin SD2 (Figure 6A; Movie S5), it must correspond to the B rather than to the C state of tropomyosin. In order to move from this position to the M state, the position of tropomyosin in our cryo-EM structure, tropomyosin needs to be slightly rotated and shifted by ~23 Å (Figures 5 and 6B; Movie S5). This corresponds to an azimuthal rotation of ~31.5° and results in an overall upward shift of tropomyosin along the filament (Figure 5; Movie S6). In comparison to the model of Li et al. (2011), the torsion angle of tropomyosin does not significantly change, but its radius is slightly decreased (Figure 5).

The large size of the azimuthal rotation also suggests that we observe a shift from the B to the M state rather than from the C to the M state. Our results strongly suggest that tropomyosin undergoes mainly sliding instead of rolling movements on F-actin. Because troponin is missing in both the model of Li et al. (2011) and our pseudoatomic model, the position and movement of tropomyosin may not reflect the situation in sarcomeres, where troponin regulates the position of tropomyosin, but

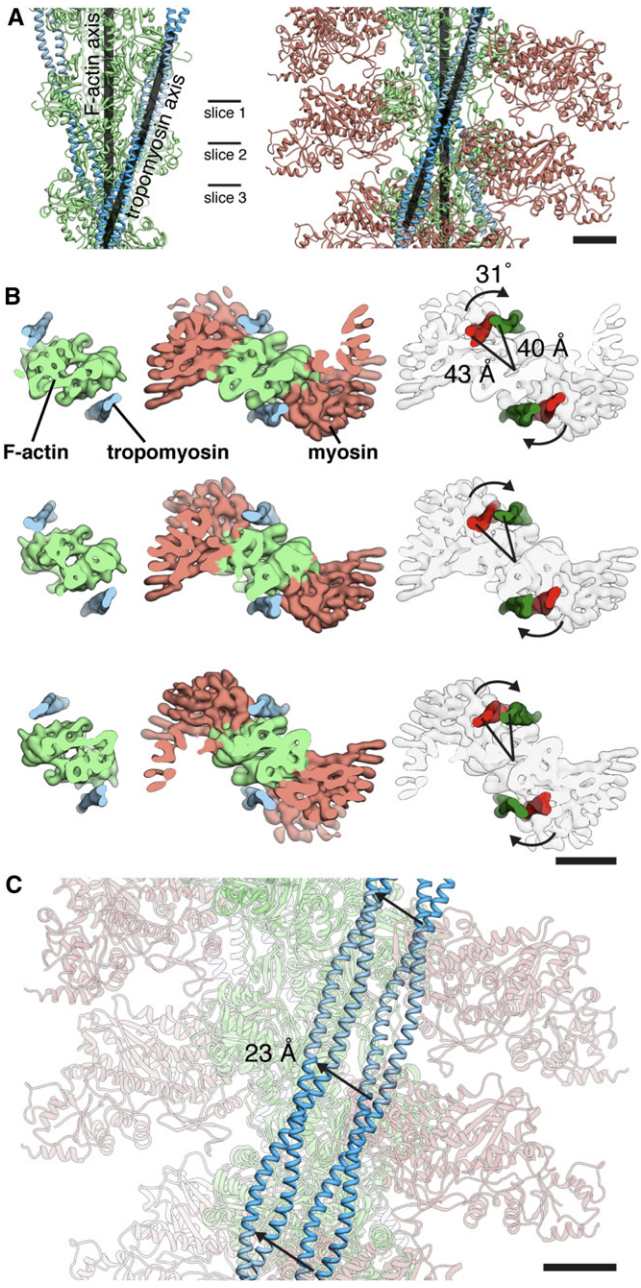

Figure 5. Tropomyosin in the B and M State

(A) Comparison of the actin-tropomyosin model when tropomyosin in its B state (Li et al., 2011) (left) with the ATM model when tropomyosin is in the M state (right) is shown. The axis of tropomyosin and the actin filament are depicted as black bars. The angle between the tropomyosin filament and the actin filament remains unchanged upon myosin binding at ~20°. Scale bar, 2.5 nm.

(B) The density of actin-tropomyosin by Li et al. (2011) was calculated at 8 Å resolution and compared with the ATM cryo-EM structure. Depicted are slices through the filament at the three positions indicated by vertical markers in (A). Upon myosin binding the position of tropomyosin is rotated azimuthally by ~31° as indicated by the arrows. In addition to the rotation, the radial position of tropomyosin is reduced from 43 to 40 Å. Scale bar, 5 nm.

(C) Overlay of the two states depicted in (A) with actin and myosin faded is presented. Displacement of tropomyosin can be described as a shift along the surface of the actin filament with additional lateral movement. MyoE, actin, and tropomyosin are salmon, light green, and blue, respectively. Scale bar, 2.5 nm.

See also Movies S5 and S6.

could more closely resemble the interaction between the proteins in nonmuscle cells.

Model for Myosin Binding and the Myosin Power Stroke

Our pseudoatomic model provides important insights into the actin-myosin-tropomyosin interaction. Although the structural record is by no means complete for the sequence of events associated with myosin binding, the actin-catalyzed release of hydrolysis products, and the power stroke, we can use the information provided by our atomic models of myoE in the prepower stroke and rigor states to define critical steps in the process and suggest the following mechanism.

Because our models show that the L50 subdomain and loop 3 are the most invariant regions between myosin in the prepower stroke and the rigor state (Figures 4D–4F), we propose that myosin initially binds mainly via this region to F-actin. In contrast to the other binding sites on actin, the ones for the L50 subdomain and loop 3 only exist on F-actin because it is formed by the interface of two actins. Initial binding in this region might therefore also serve for myosin to discriminate between G- and F-actin.

In order for myosin to bind to tropomyosin-decorated actin in the absence of troponin, myosin needs to rotate azimuthally by 20° away from its final binding position (Figure 6C). This mode of binding is consistent with previously described interactions of loop 2 with actin (Furch et al., 1998; Murphy and Spudich, 1999) and the aforementioned described flexibility of the converter domain. A subsequent rotation and closure of myosin's 50 kDa cleft, which is induced by strong interactions between actin and myosin, will push tropomyosin further aside by about 23 Å (Figure 6C; Movie S7A). At the same time tropomyosin diffusion from the actomyosin complex is prevented by Gestalt binding and electrostatic interactions. In this model an oscillation of tropomyosin between M and B states, as described by McKillop and Geeves (1993), is not necessary. However, if myosin cannot rotate in this manner, its binding to actin will be sterically hindered as long as tropomyosin remains in the B state and oscillation of tropomyosin is required (Movie S7B).

Whereas individual actin monomers and monomer contacts within the filament do not significantly change their conformation during the interaction with myosin, myosin undergoes large changes (Figure 7). A rotation of U50 toward actin, and the L50 subdomain closes the 50 kDa cleft (Figures 4D, 4E, 7A, 7C, and S6A; Movie S3). The resulting structural changes are then transmitted to actin-distal myosin domains (Figures 7D, 7E, S6B, and S6C). This leads to a compression of the transducer domain, which is further amplified by the L50 subdomain (Figures 7F and S6D). As a result, the N-terminal domain of myosin is compressed like a spring, which relaxes by a rotation only after P_i and ADP are released, resulting in a large swing of the lever arm (Figures 7G, 7H, S6E, and S6F). This is the mechanistic basis for the amplification of the movement induced by

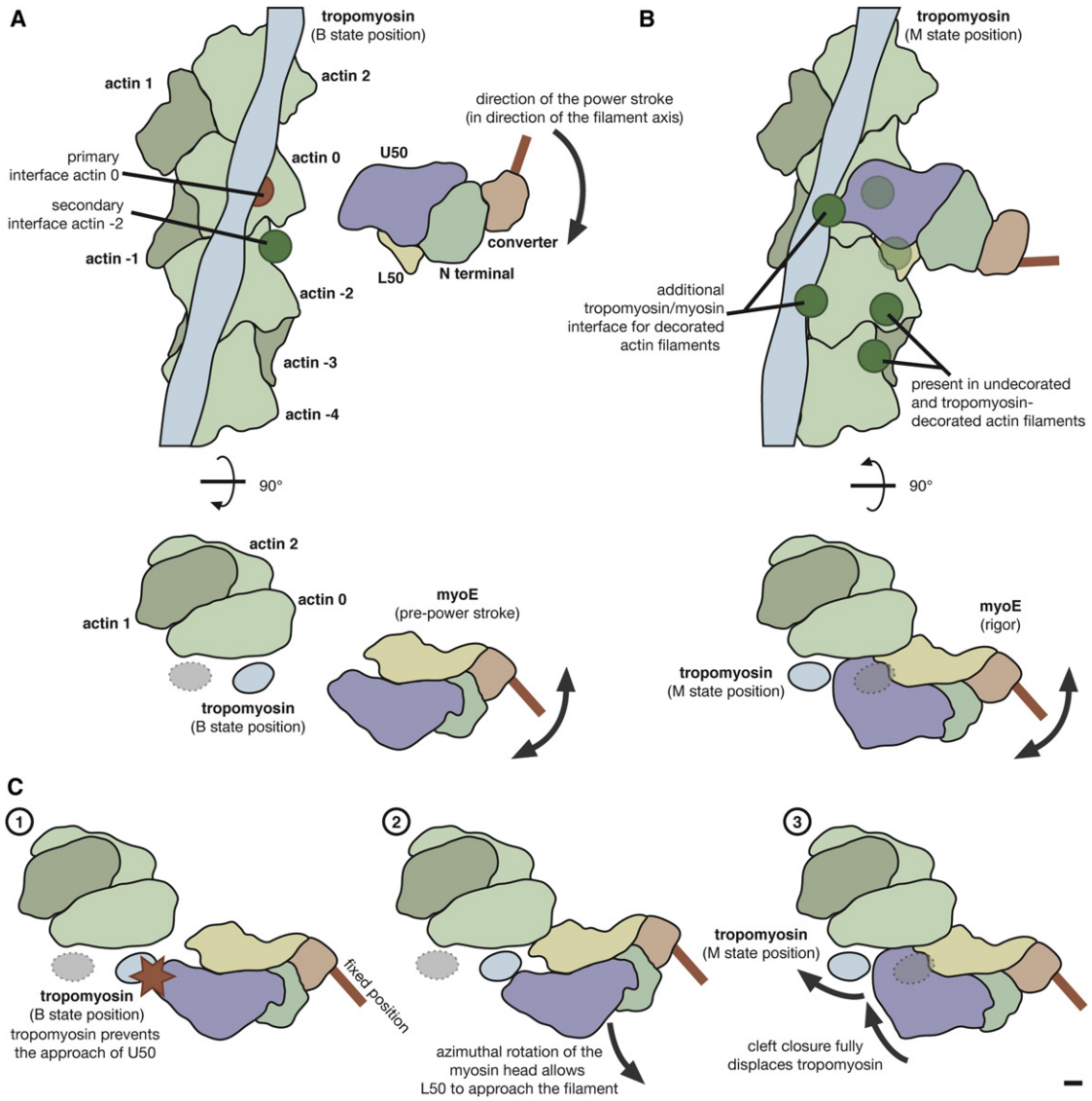

Figure 6. Model of Myosin Binding and Displacement of Tropomyosin on Actin Filaments in the Absence of Troponin

(A) Tropomyosin in its B state obscures a large part of the myosin-binding site on actin.

(B and C) A shift of tropomyosin from its B to M state exposes the myosin-binding sites and allows myosin to attach to actin. This results also in an additional interface between tropomyosin and myosin. Either tropomyosin oscillates between its B and M state in the absence of troponin, or (C) the myosin motor domain rotates azimuthally to the axis of actin by about 20°, so that the L50 subdomain of myosin can interact with myosin-binding sites on actin, which are not occluded by tropomyosin. Closure of the 50 kDa cleft and an azimuthal rotation of myosin fully move tropomyosin to its position in the M state. Scale bar, 1 nm.

See also Movie S7.

the release of energy obtained from ATP hydrolysis by interaction with myosin at the L50 and U50 subdomain. The power stroke can only be fully completed after Mg^{2+}-ADP has been released from the nucleotide-binding pocket. A detailed description of this process is given in Figure 7.

Obviously, more evidence is needed before our model for myosin binding and the myosin power stroke can be regarded as established. Thus, additional structures of intermediate states, such as the weakly and strongly bound ADP states, are needed.

Implications for Myopathies

Mutations of the genes encoding human tropomyosin, actin, and myosin isoforms are in part associated with familial hypertrophic CM or nemaline rod myopathy (Bonne et al., 1998). Our subnanometer-resolution structure of the ATM complex allows a clear assignment of residues contributing to the ATM interface (Table S1). Mutations associated with severe myopathies are distributed all over the interface, where key residues are conserved across isoform and species boundaries (Figure 3E). Disease-causing mutations disrupt both electrostatic and

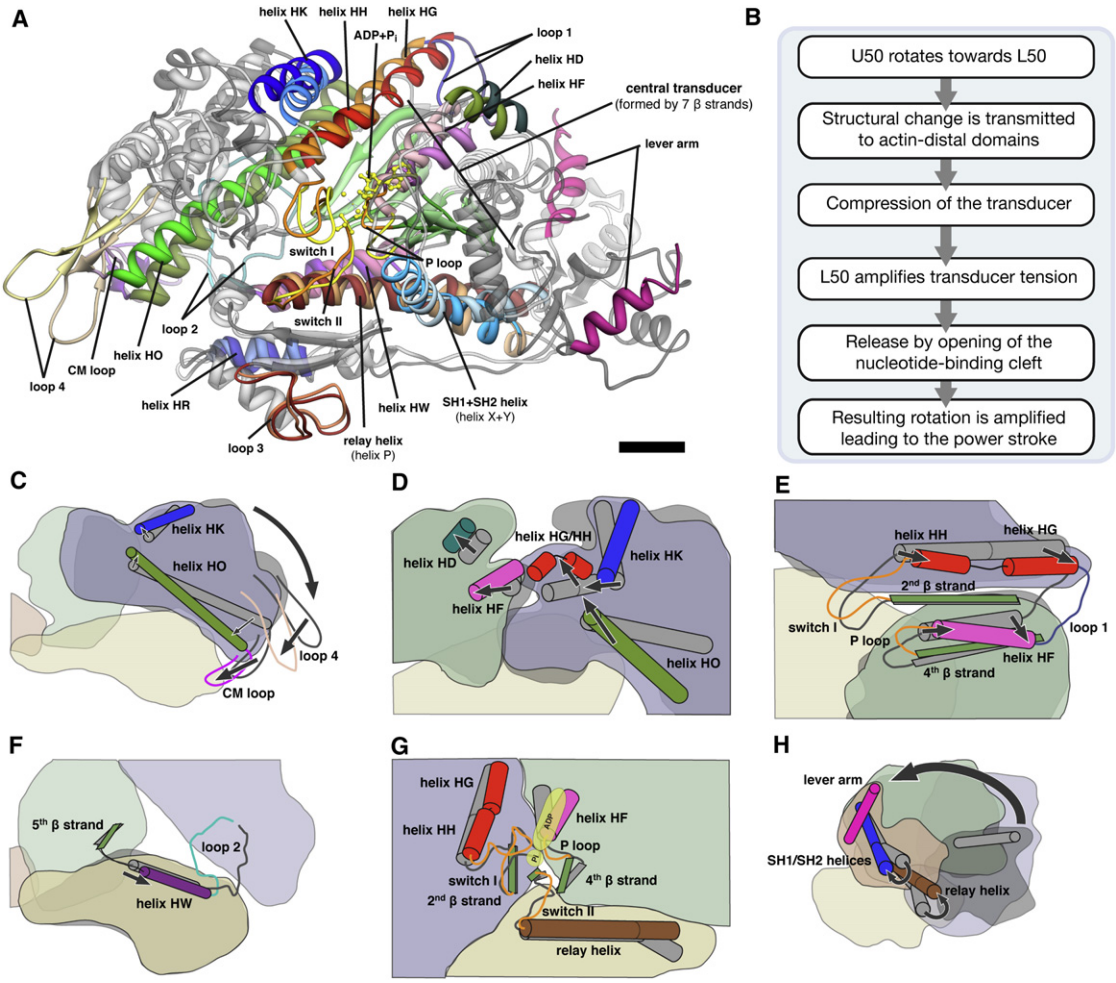

Figure 7. Model of Actin-Induced Force Generation in Myosin

(A) Overview of structural changes in myosin needed for transition from prepower stroke (light gray) to rigor state (dim gray) is illustrated. Helices and loops associated with important conformational changes are highlighted in color (helix HK, dark and light blue; helix HG, red and orange; helix HH, olive and green; helix HW, purple and pink; relay helix, dark and light brown; loop 1, dark and light lilac; loop 2, dark and light cyan; switch I/II and P loop, orange and yellow; transducer β sheets, green and light green; SH1+SH2 helix, blue and light blue; lever arm, magenta and dark magenta; rigor and prepower stroke positions, respectively) and labeled.

(B–H) Flow chart and (C–H) schematic views describing the model of the power stroke are demonstrated. See Figure 1B for an overview of myoE subdomains. (C) Binding of the CM loop and loop 4 to actin induces a rotation of the U50 subdomain toward actin, which results in the closure of the 50 kDa cleft. Due to this rotation helices HO and HK are pushed in a seesaw-like mechanism toward the N-terminal domain. (D) The concerted action of helices HO and HK forces helices HG and HH to bulge and shift, which successively displaces helices HF and HD of the N-terminal domain. (E) These displacements of helices are directly transmitted to switch I, loop 1, the P loop, and the fourth β strand of the central transducer sheet. (F) Induced by a strong binding of loop 2 to actin, the HW helix of the L50 subdomain is pulled toward actin, transmitting the force to the fifth β strand. (G) P_i and ADP binding by switch I is destabilized, and the back door for P_i is opened. (H) Release of P_i and ADP results in a rotation of the N-terminal subdomain, which pulls on the SH1 and SH2 helices. This leads to a rotation of the converter domain accompanied by a stretching of the kinked relay helix and a large swing of the lever arm. Scale bar, 1 nm.

See also Figure S6.

hydrophobic contacts, thereby directly perturbing the interactions between actin, tropomyosin and myosin. Our structure of the ATM complex could serve as a strong foundation to address the role of individual mutations in the genesis of myopathies. Moreover, the elucidation of key interactions in the ATM interphase will facilitate the development of drugs that target the mutated ATM complex. A drug-based approach is very attractive due to the highly localized effects of the disease-causing mutations, which can be linked to the isoform-specific composition displayed by ATM complexes throughout vertebrate cells and tissues.

EXPERIMENTAL PROCEDURES

Detailed experimental procedures can be found in the Extended Experimental Procedures.

Filament Preparation

F-actin was prepared from rabbit skeletal muscle. Recombinant tropomyosin and myoE were purified from *E. coli* and *Dictyostelium discoideum* cells, respectively. Thin filaments were prepared by mixing F-actin (0.1 mg ml^{-1}) with tropomyosin at a molar ratio of 1:7 in 5 mM HEPES-OH (pH 7.2), 100 mM KCl, 2 mM $MgCl_2$, 50 mM glutamine, and 50 mM arginine. The full complex was prepared by additionally adding myoE at slight molar excess to the thin filaments. The resulting filament suspension was used for cryo-EM within 15 min to minimize bundling.

Electron Microscopy

For cryo-EM the sample was diluted 10-fold, applied to C-Flat R2/1 holey carbon grids (Protochips), and vitrified. Filaments were imaged with a JEM-3200FSC electron microscope (JEOL) at an acceleration voltage of 200kV operated at liquid nitrogen temperature. An in-column omega energy filter was used to improve image contrast by zero-loss filtering with a slit-width of 12 eV. Micrographs were recorded at 169,644× magnification with an 8k × 8k TemCam-F816 CMOS camera (TVIPS) under minimal dose conditions (15–20 $e^{-}/Å^2$) resulting in an effective pixel size of 0.92 Å on the specimen scale.

Image Processing

The SPARX software (Hohn et al., 2007) was used for all image-processing steps, with the exception of the initial defocus determination, which was done using CTFFIND3 (Mindell and Grigorieff, 2003). Decorated filaments were identified using K-means clustering and processed according to the SPARX implementation of the iterative helical real-space refinement scheme (Egelman, 2000). Structural heterogeneity found in myosin was separated using a codimensional PCA modified to work with structures having helical symmetry (Behrmann et al., 2012).

Fitting

Atomic models of F-actin (Fujii et al., 2010) (PDB 3MFP), myoE (Kollmar et al., 2002) (PDB 1LKX), and tropomyosin (Li et al., 2011) were fit into the EM volumes first by rigid-body using Chimera (Pettersen et al., 2004) and then by flexible fitting with DireX (Schröder et al., 2007). Eigenvector analysis of the models was done using the Bio3d package in R (Grant et al., 2006).

ACCESSION NUMBERS

The coordinates and structure factors for the actin-myosin-tropomyosin EM reconstructions and the atomic models have been deposited in the EM Data Bank and the RCSB Protein Data Bank under accession codes EMD-1987-1990, and 4a7n, 4a7l, 4a7h, and 4a7f, respectively.

SUPPLEMENTAL INFORMATION

Supplemental Information includes Extended Experimental Procedures, six figures, one table, and seven movies and can be found with this article online at http://dx.doi.org/10.1016/j.cell.2012.05.037.

ACKNOWLEDGMENTS

We are grateful to R.S. Goody for continuous support and thank him and C. Ungermann for useful comments on the manuscript. We thank O. Hofnagel for assistance at the electron microscope and I. Vetter for help with the installation of SPARX. We are grateful to G. Schröder for helpful comments on the use of DireX and W. Lehman for providing the tropomyosin model in the B state. We thank K. Chinthalapudi, R. Diensthuber, S.M. Heissler, and M. Taft for providing purified proteins. This work was supported by the "Deutsche Forschungsgemeinschaft" Grants RA 1781/1-1 (to S.R.), MA 807/17-2 (to H.G.M.), MA 1081/11-2 (to. D.J.M.), the "Fonds der chemischen Industrie" Grant 684052 (to E.B.), funding from the European Union Seventh Framework Programme (FP7/2007-2011) under grant agreement number 228971 (Molecular Motors-based Nano Devices-MONAD) (to D.J.M.), the NIH Grants GM U54 094598 and GM R01 60635 (to P.A.P.), and the Max Planck Society (to S.R. and E.B.).

M.M. and. H.G.M. purified proteins; E.B. and H.G.M. screened samples and collected EM data; E.B., P.A.P., and S.R. processed, refined, and analyzed EM data; E.B. and S.R. wrote the paper; and D.J.M. and S.R. designed the study. D.J.M. cowrote the paper. All authors discussed the results and commented on the manuscript.

Received: January 20, 2012
Revised: March 13, 2012
Accepted: May 20, 2012
Published: July 19, 2012

REFERENCES

Behrmann, E., Tao, G., Stokes, D.L., Egelman, E.H., Raunser, S., and Penczek, P.A. (2012). Real-space processing of helical filaments in SPARX. J. Struct. Biol. *177*, 302–313.

Bonne, G., Carrier, L., Richard, P., Hainque, B., and Schwartz, K. (1998). Familial hypertrophic cardiomyopathy: from mutations to functional defects. Circ. Res. *83*, 580–593.

Conibear, P.B., Bagshaw, C.R., Fajer, P.G., Kovács, M., and Málnási-Csizmadia, A. (2003). Myosin cleft movement and its coupling to actomyosin dissociation. Nat. Struct. Biol. *10*, 831–835.

Coureux, P.D., Wells, A.L., Ménétrey, J., Yengo, C.M., Morris, C.A., Sweeney, H.L., and Houdusse, A. (2003). A structural state of the myosin V motor without bound nucleotide. Nature *425*, 419–423.

Coureux, P.D., Sweeney, H.L., and Houdusse, A. (2004). Three myosin V structures delineate essential features of chemo-mechanical transduction. EMBO J. *23*, 4527–4537.

Dürrwang, U., Fujita-Becker, S., Erent, M., Kull, F.J., Tsiavaliaris, G., Geeves, M.A., and Manstein, D.J. (2006). *Dictyostelium* myosin-IE is a fast molecular motor involved in phagocytosis. J. Cell Sci. *119*, 550–558.

Eaton, B.L. (1976). Tropomyosin binding to F-actin induced by myosin heads. Science *192*, 1337–1339.

Ebashi, S., Endo, M., and Otsuki, I. (1969). Control of muscle contraction. Q. Rev. Biophys. *2*, 351–384.

Egelman, E.H. (2000). A robust algorithm for the reconstruction of helical filaments using single-particle methods. Ultramicroscopy *85*, 225–234.

Fujii, T., Iwane, A.H., Yanagida, T., and Namba, K. (2010). Direct visualization of secondary structures of F-actin by electron cryomicroscopy. Nature *467*, 724–728.

Furch, M., Geeves, M.A., and Manstein, D.J. (1998). Modulation of actin affinity and actomyosin adenosine triphosphatase by charge changes in the myosin motor domain. Biochemistry *37*, 6317–6326.

Furch, M., Remmel, B., Geeves, M.A., and Manstein, D.J. (2000). Stabilization of the actomyosin complex by negative charges on myosin. Biochemistry *39*, 11602–11608.

Galkin, V.E., Orlova, A., Schröder, G.F., and Egelman, E.H. (2010). Structural polymorphism in F-actin. Nat. Struct. Mol. Biol. *17*, 1318–1323.

Geeves, M.A., and Halsall, D.J. (1986). The dynamics of the interaction between myosin subfragment 1 and pyrene-labelled thin filaments, from rabbit skeletal muscle. Proc. R. Soc. Lond. B Biol. Sci. *229*, 85–95.

Geisterfer-Lowrance, A.A., Kass, S., Tanigawa, G., Vosberg, H.P., McKenna, W., Seidman, C.E., and Seidman, J.G. (1990). A molecular basis for familial hypertrophic cardiomyopathy: a beta cardiac myosin heavy chain gene missense mutation. Cell *62*, 999–1006.

Giese, K.C., and Spudich, J.A. (1997). Phenotypically selected mutations in myosin's actin binding domain demonstrate intermolecular contacts important for motor function. Biochemistry *36*, 8465–8473.

Goodson, H.V., Warrick, H.M., and Spudich, J.A. (1999). Specialized conservation of surface loops of myosin: evidence that loops are involved in determining functional characteristics. J. Mol. Biol. *287*, 173–185.

Grant, B.J., Rodrigues, A.P., ElSawy, K.M., McCammon, J.A., and Caves, L.S. (2006). Bio3d: an R package for the comparative analysis of protein structures. Bioinformatics *22*, 2695–2696.

Hansen, J.E., Marner, J., Pavlov, D., Rubenstein, P.A., and Reisler, E. (2000). Structural transition at actin's N-terminus in the actomyosin cross-bridge cycle. Biochemistry *39*, 1792–1799.

Hohn, M., Tang, G., Goodyear, G., Baldwin, P.R., Huang, Z., Penczek, P.A., Yang, C., Glaeser, R.M., Adams, P.D., and Ludtke, S.J. (2007). SPARX, a new environment for cryo-EM image processing. J. Struct. Biol. *157*, 47–55.

Holmes, K.C., and Lehman, W. (2008). Gestalt-binding of tropomyosin to actin filaments. J. Muscle Res. Cell Motil. *29*, 213–219.

Holmes, K.C., Angert, I., Kull, F.J., Jahn, W., and Schröder, R.R. (2003). Electron cryo-microscopy shows how strong binding of myosin to actin releases nucleotide. Nature *425*, 423–427.

Holthauzen, L.M., Corrêa, F., and Farah, C.S. (2004). Ca2+-induced rolling of tropomyosin in muscle thin filaments: the alpha- and beta-band hypothesis revisited. J. Biol. Chem. *279*, 15204–15213.

Houdusse, A., Szent-Gyorgyi, A.G., and Cohen, C. (2000). Three conformational states of scallop myosin S1. Proc. Natl. Acad. Sci. USA *97*, 11238–11243.

Huxley, H.E., Faruqi, A.R., Bordas, J., Koch, M.H., and Milch, J.R. (1980). The use of synchrotron radiation in time-resolved X-ray diffraction studies of myosin layer-line reflections during muscle contraction. Nature *284*, 140–143.

Irving, M., Piazzesi, G., Lucii, L., Sun, Y.B., Harford, J.J., Dobbie, I.M., Ferenczi, M.A., Reconditi, M., and Lombardi, V. (2000). Conformation of the myosin motor during force generation in skeletal muscle. Nat. Struct. Biol. *7*, 482–485.

Joel, P.B., Trybus, K.M., and Sweeney, H.L. (2001). Two conserved lysines at the 50/20-kDa junction of myosin are necessary for triggering actin activation. J. Biol. Chem. *276*, 2998–3003.

Kim, E., Bobkova, E., Hegyi, G., Muhlrad, A., and Reisler, E. (2002). Actin cross-linking and inhibition of the actomyosin motor. Biochemistry *41*, 86–93.

Klein, J.C., Burr, A.R., Svensson, B., Kennedy, D.J., Allingham, J., Titus, M.A., Rayment, I., and Thomas, D.D. (2008). Actin-binding cleft closure in myosin II probed by site-directed spin labeling and pulsed EPR. Proc. Natl. Acad. Sci. USA *105*, 12867–12872.

Kollmar, M., Dürrwang, U., Kliche, W., Manstein, D.J., and Kull, F.J. (2002). Crystal structure of the motor domain of a class-I myosin. EMBO J. *21*, 2517–2525.

Lehman, W., Vibert, P., Uman, P., and Craig, R. (1995). Steric-blocking by tropomyosin visualized in relaxed vertebrate muscle thin filaments. J. Mol. Biol. *251*, 191–196.

Li, X.E., Lehman, W., and Fischer, S. (2010). The relationship between curvature, flexibility and persistence length in the tropomyosin coiled-coil. J. Struct. Biol. *170*, 313–318.

Li, X.E., Tobacman, L.S., Mun, J.Y., Craig, R., Fischer, S., and Lehman, W. (2011). Tropomyosin position on F-actin revealed by EM reconstruction and computational chemistry. Biophys. J. *100*, 1005–1013.

Lymn, R.W., and Taylor, E.W. (1971). Mechanism of adenosine triphosphate hydrolysis by actomyosin. Biochemistry *10*, 4617–4624.

McKillop, D.F., and Geeves, M.A. (1993). Regulation of the interaction between actin and myosin subfragment 1: evidence for three states of the thin filament. Biophys. J. *65*, 693–701.

Miller, C.J., Wong, W.W., Bobkova, E., Rubenstein, P.A., and Reisler, E. (1996). Mutational analysis of the role of the N terminus of actin in actomyosin interactions. Comparison with other mutant actins and implications for the cross-bridge cycle. Biochemistry *35*, 16557–16565.

Milligan, R.A. (1996). Protein-protein interactions in the rigor actomyosin complex. Proc. Natl. Acad. Sci. USA *93*, 21–26.

Milligan, R.A., and Flicker, P.F. (1987). Structural relationships of actin, myosin, and tropomyosin revealed by cryo-electron microscopy. J. Cell Biol. *105*, 29–39.

Mindell, J.A., and Grigorieff, N. (2003). Accurate determination of local defocus and specimen tilt in electron microscopy. J. Struct. Biol. *142*, 334–347.

Murphy, C.T., and Spudich, J.A. (1999). The sequence of the myosin 50-20K loop affects Myosin's affinity for actin throughout the actin-myosin ATPase cycle and its maximum ATPase activity. Biochemistry *38*, 3785–3792.

Oda, T., Iwasa, M., Aihara, T., Maéda, Y., and Narita, A. (2009). The nature of the globular- to fibrous-actin transition. Nature *457*, 441–445.

Pettersen, E.F., Goddard, T.D., Huang, C.C., Couch, G.S., Greenblatt, D.M., Meng, E.C., and Ferrin, T.E. (2004). UCSF Chimera—a visualization system for exploratory research and analysis. J. Comput. Chem. *25*, 1605–1612.

Rayment, I., Holden, H.M., Whittaker, M., Yohn, C.B., Lorenz, M., Holmes, K.C., and Milligan, R.A. (1993). Structure of the actin-myosin complex and its implications for muscle contraction. Science *261*, 58–65.

Reubold, T.F., Eschenburg, S., Becker, A., Kull, F.J., and Manstein, D.J. (2003). A structural model for actin-induced nucleotide release in myosin. Nat. Struct. Biol. *10*, 826–830.

Sasaki, N., Asukagawa, H., Yasuda, R., Hiratsuka, T., and Sutoh, K. (1999). Deletion of the myopathy loop of *Dictyostelium* myosin II and its impact on motor functions. J. Biol. Chem. *274*, 37840–37844.

Schröder, G.F., Brunger, A.T., and Levitt, M. (2007). Combining efficient conformational sampling with a deformable elastic network model facilitates structure refinement at low resolution. Structure *15*, 1630–1641.

Schröder, R.R., Manstein, D.J., Jahn, W., Holden, H., Rayment, I., Holmes, K.C., and Spudich, J.A. (1993). Three-dimensional atomic model of F-actin decorated with *Dictyostelium* myosin S1. Nature *364*, 171–174.

Sparrow, J.C., Nowak, K.J., Durling, H.J., Beggs, A.H., Wallgren-Pettersson, C., Romero, N., Nonaka, I., and Laing, N.G. (2003). Muscle disease caused by mutations in the skeletal muscle alpha-actin gene (ACTA1). Neuromuscul. Disord. *13*, 519–531.

Splettstoesser, T., Holmes, K.C., Noé, F., and Smith, J.C. (2011). Structural modeling and molecular dynamics simulation of the actin filament. Proteins *79*, 2033–2043.

Sweeney, H.L., and Houdusse, A. (2010). Structural and functional insights into the Myosin motor mechanism. Annu. Rev. Biophys. *39*, 539–557.

Van Dijk, J., Furch, M., Lafont, C., Manstein, D.J., and Chaussepied, P. (1999). Functional characterization of the secondary actin binding site of myosin II. Biochemistry *38*, 15078–15085.

Vibert, P., Craig, R., and Lehman, W. (1997). Steric-model for activation of muscle thin filaments. J. Mol. Biol. *266*, 8–14.

Volkmann, N., Ouyang, G., Trybus, K.M., DeRosier, D.J., Lowey, S., and Hanein, D. (2003). Myosin isoforms show unique conformations in the actin-bound state. Proc. Natl. Acad. Sci. USA *100*, 3227–3232.